

Fast, Accurate and Lightweight Super-Resolution with Neural Architecture Search

Xiangxiang Chu¹, Bo Zhang¹, Hailong Ma¹, Ruijun Xu¹, Jixiang Li¹ and Qingyuan Li²

¹Xiaomi AI

²Xiaomi IOT

{chuxiangxiang, zhangbo11, mahailong, xuruijun, lijixiang, liqingyuan}@xiaomi.com

Abstract

Deep convolution neural networks demonstrate impressive results in super-resolution domain. An ocean of researches concentrate on improving peak signal noise ratio (PSNR) by using deeper and deeper layers, which is not friendly to constrained resources. Pursuing a trade-off between restoration capacity and simplicity of a model is still non-trivial by now. Recently, more contributions are devoted to this balance and our work is focusing on improving it further with automatic neural architecture search. In this paper, we handle super-resolution using multi-objective approach and propose an elastic search method involving both macro and micro aspects based on a hybrid controller of evolutionary algorithm and reinforcement learning. Quantitative experiments can help to draw a conclusion that the models generated by our methods are very competitive than and even dominate most of state-of-the-art super-resolution methods with different levels of FLOPS.

1 Introduction and Related Works

As a classical task in computer vision, single image super-resolution (SISR) is aimed to restore a high-resolution image from a degraded low-resolution one, which is known as an ill-posed inverse procedure. Deep learning has aroused great interest of research from various areas, which achieved impressive reconstruction result. Most of the recent works on SISR have shifted their approaches to deep learning, and they have surpassed other SISR algorithms with big margins [Dong *et al.*, 2014; Kim *et al.*, 2016a; He *et al.*, 2016; Ahn *et al.*, 2018].

Nonetheless, these human-designed models are tangible to fine tune or to compress. Meantime, neural architecture search has produced dominating models in classification tasks [Zoph and Le, 2016; Zoph *et al.*, 2017]. Following this trend, a novel work by [Chu *et al.*, 2019] has shed light on SISR task with a reinforced evolutionary search method, which has achieved results outperforming some notable networks including VDSR [Kim *et al.*, 2016a].

In this paper, we dive deeper into the SISR task with elastic neural architecture search, hitting a record comparable to

CARN and CARN-M [Ahn *et al.*, 2018]¹. Our main contributions can be summarized in the following four aspects,

- releasing several fast, accurate and lightweight super-resolution architectures and models, which are highly competitive with recent state-of-the-art methods (some even dominating),
- performing elastic search by combining macro with micro space on the level of cells to boost representative capacity,
- building super-resolution as a constrained multi-objective optimization problem and applying a hybrid model generation method to balance exploration and exploitation,
- producing high-quality models that can meet various requirements given different constraints within a single run.

2 Pipeline Architecture

Like most of NAS approaches, our pipeline contains three principle ingredients: search space supporting elastic search, a hybrid model generator and a model evaluator based on incomplete training. Their details will be explained successively in the following sections.

Like [Lu *et al.*, 2018; Chu *et al.*, 2019], we also apply NS-GAII [Deb *et al.*, 2002] to solve the multi-objective problem. Unlike [Lu *et al.*, 2018], we use a hybrid controller and cell based elastic search space. Unlike [Chu *et al.*, 2019], we perform both macro and micro search.

We take into account three objectives for super-resolution task,

- quantitative metric to reflect models' performances (PSNR),
- quantitative metric to evaluate models' computing cost (multi-adds),
- number of parameters.

In addition, we consider the following constraints,

- minimal PSNR based on perceptual result,
- maximal multi-adds regarding constrained resource.

¹Our models are released at <https://github.com/falsr/FALSR>.

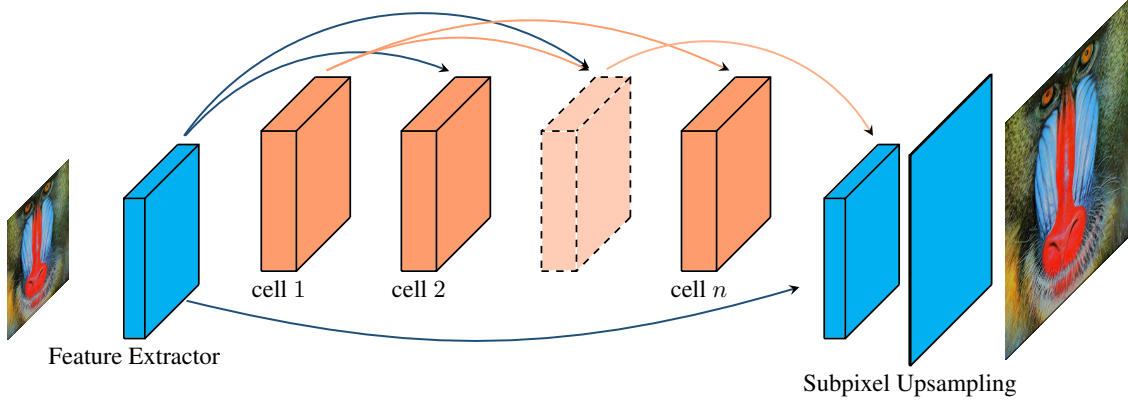


Figure 1: Neural Architecture of Super-Resolution (the arrows denote skip connections).

3 Elastic Search Space

Our search space is designed to perform both macro and micro search. While the former is aimed to search backbone connections for different cell blocks to play a role of combining selected levels of features, the latter is used to choose good cells within each cell block, which can be viewed as feature extraction selector. In addition, we use cell block as our minimum search element for two reasons. One is design flexibility, another is good capacity of representing various architectures.

In general, super resolution task can be divided into three sub-procedures by logic: feature extraction, nonlinear mapping and restoration. Since most of deep learning approaches concentrate on the second part, we design our search space to perform this mapping while fix other parts. Figure 1 depicts our main stream for super resolution. Obviously, a complete model contains a fixed feature extractor(2D convolution with $32\ 3 \times 3$ filters), n cell blocks which are defined by the micro and connected by the macro search, sub-pixel based up-sampling and restoration².

3.1 Cell Level Micro Search Space

For simplicity, all cell blocks share a single cell search space S . In specific, the micro search space for each cell block contains the following elements:

- convolutions: 2D convolution, grouped convolution with group in $\{2, 4\}$, inverted bottleneck block with expansion rate 2,
- channels: $\{16, 32, 48, 64\}$,
- kernels: $\{1, 3\}$,
- in-cell residual connections: $\{\text{True}, \text{False}\}$,
- repeated blocks: $\{1, 2, 4\}$.

Therefore, the size of micro space for n cell blocks is 192^n .

3.2 Macro Search Space Among Cells

The macro search defines the connections among different cell blocks. In specific, for the i th cell block CB_i , there are

²Here, the up-sampling contains a 2D convolution with $32\ 3 \times 3$ filters. A 3×3 convolutions with one filter and unit stride.

$n + 1 - i$ connections to be chosen to build the information flow from the input of CB_i to its following cell blocks³. Furthermore, we use c_i^j to represent the path from input of CB_i to CB_j . And $c_i^j = 1$ if there is a connection path, otherwise 0. Therefore, the size of macro space for n cell blocks is $2^{\frac{n(n+1)}{2}}$. In summary, the size of total space is $192^n \times 2^{\frac{n(n+1)}{2}}$.

4 Model Generator

Our model generator is a hybrid controller involving both reinforcement learning and evolutionary algorithms. EA controls the outer loop and reinforcement learning is used to bring in exploitation. In specific, the outer loop is controlled by NSGA-II [Deb *et al.*, 2002], which contains four sub-procedures: population initialization, selection, cross-over and mutation. To avoid verbosity, we only cover differences from NSGA-II.

4.1 Model Meta Encoding

One model is defined by two parts, forward-connected cells and their information connections. As [Chu *et al.*, 2019], we use operators' indexes located in the operator set to encode the former part, and use a nested list to depict the latter one. Given a model M with n cells, its corresponding chromosomes can be depicted by (M_{mic}, M_{mac}) , where M_{mic} and M_{mac} are defined as follows,

$$M_{mic} = (x_1, x_2, \dots, x_n) \quad (1)$$

$$M_{mac} = (c_1^{1:n}, c_2^{2:n}, \dots, c_n^n) \quad (2)$$

$$c_i^{i:n} = (c_i^i, c_i^{i+1}, \dots, c_i^n)$$

4.2 Initialization

Here, we initialize N populations and we emphasize the cell diversities. Therefore, to generate a model, we randomly sample a cell from S and repeated it n times. If N is larger than the size of S , we randomly sample a model.

As for connections, we use a category distribution to generate paths. We sample p by $p \sim \text{Uniform}(0, 1)$ and build

³ i starts with 1.

connections based on the following rules,

$$\begin{cases} \text{random connections} & 0 \leq p < p_r \\ \text{dense connections} & p_r \leq p < p_r + p_{den} \\ \text{no connections} & p_r + p_{den} \leq p < 1 \end{cases} \quad (3)$$

4.3 Tournament Selection

We calculate the crowding distance as [Chu and Yu, 2018; Chu *et al.*, 2019] to distribute our models more uniformly, and use tournament selection ($k = 2$) to control the evolution pressure.

4.4 Cross Over

To encourage exploration, we perform cross-over across both macro and micro spaces simultaneously. In particular, we apply single-point cross-over for both parts. Given two models $A (M_{mic(A)}, M_{mac(A)})$ and $B (M_{mic(B)}, M_{mac(B)})$, the chromosome C can be generated as,

$$\begin{aligned} M_{mic(C)} &= (x_{1A}, x_{2A}, \dots, x_{iB}, \dots, x_{nA}) \\ M_{mac(C)} &= (c_{1A}^{1:n}, c_{2A}^{2:n}, \dots, c_{jB}^{j:n}, \dots, c_{nA}^n) \end{aligned} \quad (4)$$

where i and j are chosen positions for micro and macro genes respectively. Informally speaking, cross over procedure contributes more exploitation than exploration.

4.5 Mutation

We apply a category distribution to balance exploration and exploitation.

Exploration

To encourage exploration, we combine random mutation with roulette wheel selection (RWS). Since we treat super-resolution as a multi-objective problem, flops and number of parameters are two objectives that can be evaluated soon after model-meta data are given. In particular, we also sample from a category distribution to determine mutating strategies in this case, i.e. random mutation or mutated by roulette wheel selection to handle flops or parameters. This procedure can be written as,

$$\begin{cases} \text{random mutation} & 0 \leq p < p_{mr} \\ \text{RWS for flops} & p_{mr} \leq p < p_{mr} + p_{mf} \\ \text{RWS for params} & p_{mr} + p_{mf} \leq p < 1 \end{cases} \quad (5)$$

Whenever we need to mutate a model M by RWS, we keep M_{mac} unchanged. Since every cell shares a single operator set S , we perform RWS on S for n times in turn to generate M_{mic} . Strictly speaking, given M_{mac} , it's intractable (involving about 192^n models) to execute RWS on a complete model. Instead, we approximate it based on S (involving 192 basic operators). Besides, we scale flops and number of parameters by \log_{10} function before RWS as [Chu *et al.*, 2019]. The detailed RWS is shown in Algorithm 1.

Exploitation

To enhance exploitation, we apply a reinforcement driven mutation.

We use a neural controller to mutate, which is shown in Figure 2. In specific, the embedding features for M_{mic} are concatenated, then injected into 3 fully-connected layers to

Algorithm 1 Roulette-wheel selection for each cell

Input: fitness values x , size N

Output: selected index

$p(x) = \text{normalize}(x)$

for $i = 1$ **to** N **do**

if $p(x_i) > p_0$ **then**

$p(x_i) = p_0$

end if

end for

$p(x) = \text{normalize}(p(x))$

$target = \text{uniform_random}(), p_{acc} = 0$

for $i = 1$ **to** N **do**

$p_{acc} += p(x_i)$

if $p_{acc} > target$ **then**

return i

end if

end for

generate M_{mac} . The last layer contains $\frac{n(n+1)}{2}$ neurons to represent connections. And its output is recorded as O^{mac} .

The network parameters can be partitioned into two groups, θ^{mic} and θ^{mac} . Then the probability of selecting S_i for cell j is $p(cell_i = S_i | \theta^{mic})$ and the probability of $c_i^j = 1$ is $p(c_i^j = 1 | \theta^{mac}) = O_{(i-1)*(n+1-0.5*i)+j}^{mac}$. Thus, the gradient $g(\theta)$ can be calculated as follows:

$$\begin{aligned} g(\theta) &= -\nabla_{\theta} \left[\sum_{i=1}^n \log p(cell_i = S_i | \theta^{mic}) * R_i + \right. \\ &\quad \left. \sum_{j=1}^{n(n+1)/2} c_j \log O_j^{mac} * R_j + \right. \\ &\quad \left. (1 - c_j) \log(1 - O_j^{mac}) * R_j \right]. \end{aligned} \quad (6)$$

In Equation 6, R_i and R_j are the discounted accumulated rewards. Here, we set the discount parameter $\gamma = 1.0$.

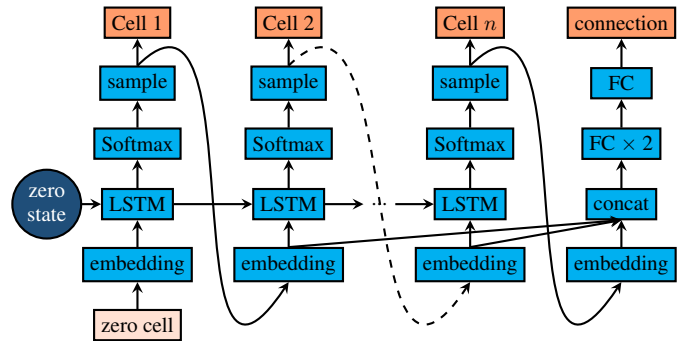


Figure 2: Controller network.

5 Evaluator

The evaluator scores generated models from the controller. In the beginning, we attempt to use a pre-trained RNN regressor to predict the performances of models by collecting some data. However, its validation error is too high, so we give up the speed-up approach. Instead, each model is trained for a relatively short time to differentiate approximately various models. In the end of incomplete training, we evaluate mean square errors of our models on test datasets.

6 Experiments

6.1 Setup

In our experiment, about 10k models are generated in total, where the population number for each iteration is 64. We profile our pipeline, so it takes us less than 3 Days on Tesla-V100 with 8 GPUs to execute the pipeline once. We use DIV2K as our training set, and use the same data augmentation tricks as [Chu *et al.*, 2019].

For incomplete training, each model is trained with batch-size 16 for 200 epochs. In addition, we apply Adam ($\beta_1 = 0.9$, $\beta_2 = 0.999$) to minimize the L_1 loss between the generated high-resolution pictures and ground truth. The learning rate is initialized as 10^{-4} and kept unchanged at this stage.

As for the full train, we choose 4 models with large crowding distance in the Pareto front between mean squared error and multi-adds, which was generated by the incomplete training stage. These models are trained based on DIV2K dataset for 24000 epochs with batch-size 16 and it takes less than 1.5 days. Moreover, we initialize convolution kernel weight w 0.02 standard deviation and 0 for bias .

6.2 Comparisons with State of the Art Super-Resolution Methods

After being fully trained, our model are compared with state-of-the-art methods across full commonly used test dataset for super-resolution. To be fair, we only consider the models with comparable flops. Therefore, too deep and large models such as RDN [Zhang *et al.*, 2018b], RCAN [Zhang *et al.*, 2018a] are excluded here. We choose PSNR and SSIM as metrics by convention [Hore and Ziou, 2010] and comparisons are made on x2 task. In addition, the multi-adds is measured based on 480×480 input.

With comparable flops as CARN [Ahn *et al.*, 2018], our model called FALSR-A (Figure 3) outperforms CARN with higher scores. In addition, it also dominates DRCN [Kim *et al.*, 2016b] and MoreMNAS-A [Chu *et al.*, 2019] across three objectives and four datasets. Moreover, it achieves higher PSNR and SSIM with fewer flops than VDSR [Kim *et al.*, 2016a], DRRN [Tai *et al.*, 2017a], CNF [Ren *et al.*, 2017] and MemNet [Tai *et al.*, 2017b].

For more light-weight version, one model called FALSR-B (Figure 4) dominates CARN-M, which means it uses fewer flops and number of parameters to score equally or higher. In addition, its architecture is interesting and the complexity of connections lies in between residual and dense connections. This means dense connection is not always the optimal way to transit information. Useless features from the lower layer

make troubles for high layers to restore high-resolution results.

Another light-weight model called FALSR-C (Figure 5), also outperforms CARN-M. This model use relatively sparse (8) connections. We suppose that this sparse flow works well with the selected cells.

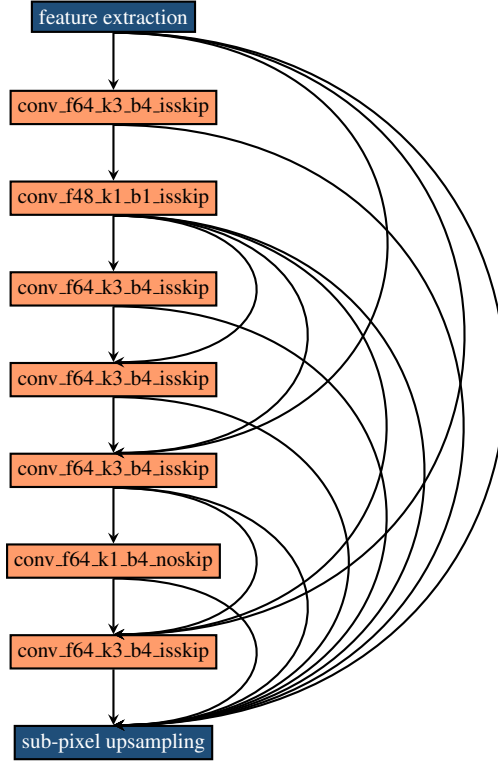


Figure 3: The model FALSR-A comparable to CARN.

Figure 6 illustrates the comparison of our models with state-of-the-art models.

Figure 8 shows the qualitative results against other methods.

6.3 Discussions

Cell Diversity

Our experiments show that cell diversity helps to achieve good results for super-resolution to as classification [Hsu *et al.*, 2018]. In fact, we train several models with repeated blocks, however, they don't outperform those models with diversity. We speculate that different types of cells can handle input features more effectively than monotonous style.

Optimal Information Flow

Perhaps, dense connection is not optimal in most cases given current technologies. In principle, dense connection has the capacity to cover other non-dense configurations, however, it's usually difficult to train the model and teach it to ignore useless information.

Model	MultAdds	Params	SET5	SET14	B100	Urban100
			PSNR/SSIM	PSNR/SSIM	PSNR/SSIM	PSNR/SSIM
SRCNN [Dong <i>et al.</i> , 2014]	52.7G	57K	36.66/0.9542	32.42/0.9063	31.36/0.8879	29.50/0.8946
FSRCNN [Dong <i>et al.</i> , 2016]	6.0G	12K	37.00/0.9558	32.63/0.9088	31.53/0.8920	29.88/0.9020
VDSR [Kim <i>et al.</i> , 2016a]	612.6G	665K	37.53/0.9587	33.03/0.9124	31.90/0.8960	30.76/0.9140
DRCN [Kim <i>et al.</i> , 2016b]	17,974.3G	1,774K	37.63/0.9588	33.04/0.9118	31.85/0.8942	30.75/0.9133
CNF [Ren <i>et al.</i> , 2017]	311.0G	337K	37.66/0.9590	33.38/0.9136	31.91/0.8962	-
LapSRN [Lai <i>et al.</i> , 2017]	29.9G	813K	37.52/0.9590	33.08/0.9130	31.80/0.8950	30.41/0.9100
DRRN [Tai <i>et al.</i> , 2017a]	6,796.9G	297K	37.74/0.9591	33.23/0.9136	32.05/0.8973	31.23/0.9188
BTSRN [Fan <i>et al.</i> , 2017]	207.7G	410K	37.75/-	33.20/-	32.05/-	31.63/-
MemNet [Tai <i>et al.</i> , 2017b]	2,662.4G	677K	37.78/0.9597	33.28/0.9142	32.08/0.8978	31.31/0.9195
SelNet [Choi and Kim, 2017]	225.7G	974K	37.89/0.9598	33.61/0.9160	32.08/0.8984	-
CARN [Ahn <i>et al.</i> , 2018]	222.8G	1,592K	37.76/0.9590	33.52/0.9166	32.09/0.8978	31.92/0.9256
CARN-M [Ahn <i>et al.</i> , 2018]	91.2G	412K	37.53/0.9583	33.26/0.9141	31.92/0.8960	31.23/0.9194
MoreMNAS-A [Chu <i>et al.</i> , 2019]	238.6G	1,039K	37.63/0.9584	33.23/0.9138	31.95/0.8961	31.24/0.9187
FALSR-A (ours)	234.7G	1,021K	37.82/0.9595	33.55/0.9168	32.12/0.8987	31.93/0.9256
FALSR-B (ours)	74.7G	326k	37.61/0.9585	33.29/0.9143	31.97/0.8967	31.28/0.9191
FALSR-C (ours)	93.7G	408k	37.66/0.9586	33.26/0.9140	31.96/0.8965	31.24/0.9187

Table 1: Comparisons with the state-of-the-art methods based on $\times 2$ super-resolution task.

Good Assumption?

Super resolution is different from feature extraction domains such as classification, which more details need restored at the level of pixel. Therefore, it scarcely applies down-sampling operations to cut down the feature dimension and needs more time to train a not too bad model than classification on CIFAR10.

Regarding the train time, we use incomplete training to differentiate various models. This strategy works well under an implicit assumption: good models (in the meaning of full train) also behave better than bad models with large probability under incomplete train. Most of deep learning tasks share this good feature luckily. For other task, we must push the incomplete train nearer to the full train.

7 Conclusions

To sum up, we presented a novel elastic method for NAS that incorporates both macro and micro search, dealing with neural architectures in multi-granularity. The result is exciting as our generated models dominate the newest state-of-the-art SR methods. Different from human-designed and single-objective NAS models, our methods can generate different tastes of models by one run, from fast, light-weight to relatively large, more accurate. Therefore, it offers a feasible way for engineers to compress existing popular human-designed models or design various levels of architectures for different constrained devices.

Our future work will focus on training a model regressor, which scores models, to speed up the pipeline.

References

[Ahn *et al.*, 2018] Namhyuk Ahn, Byungkon Kang, and Kyung-Ah Sohn. Fast, accurate, and, lightweight super-

resolution with cascading residual network. *arXiv preprint arXiv:1803.08664*, 2018.

[Choi and Kim, 2017] Jae-Seok Choi and Munchurl Kim. A deep convolutional neural network with selection units for super-resolution. In *Computer Vision and Pattern Recognition Workshops (CVPRW), 2017 IEEE Conference on*, pages 1150–1156. IEEE, 2017.

[Chu and Yu, 2018] Xiangxiang Chu and Xinjie Yu. Improved crowding distance for nsga-ii. *arXiv preprint arXiv:1811.12667*, 2018.

[Chu *et al.*, 2019] Xiangxiang Chu, Bo Zhang, Ruijun Xu, and Hailong Ma. Multi-objective reinforced evolution in mobile neural architecture search. *arXiv preprint arXiv:1901.01074*, 2019.

[Deb *et al.*, 2002] Kalyanmoy Deb, Amrit Pratap, Sameer Agarwal, and TAMT Meyarivan. A fast and elitist multi-objective genetic algorithm: Nsga-ii. *IEEE transactions on evolutionary computation*, 6(2):182–197, 2002.

[Dong *et al.*, 2014] Chao Dong, Chen Change Loy, Kaiming He, and Xiaoou Tang. Learning a deep convolutional network for image super-resolution. In *European conference on computer vision*, pages 184–199. Springer, 2014.

[Dong *et al.*, 2016] Chao Dong, Chen Change Loy, and Xiaoou Tang. Accelerating the super-resolution convolutional neural network. In *European Conference on Computer Vision*, pages 391–407. Springer, 2016.

[Fan *et al.*, 2017] Yuchen Fan, Honghui Shi, Jiahui Yu, Ding Liu, Wei Han, Haichao Yu, Zhangyang Wang, Xinchao Wang, and Thomas S Huang. Balanced two-stage residual networks for image super-resolution. In *2017 IEEE Conference on Computer Vision and Pattern Recognition Workshops (CVPRW)*, pages 1157–1164. IEEE, 2017.

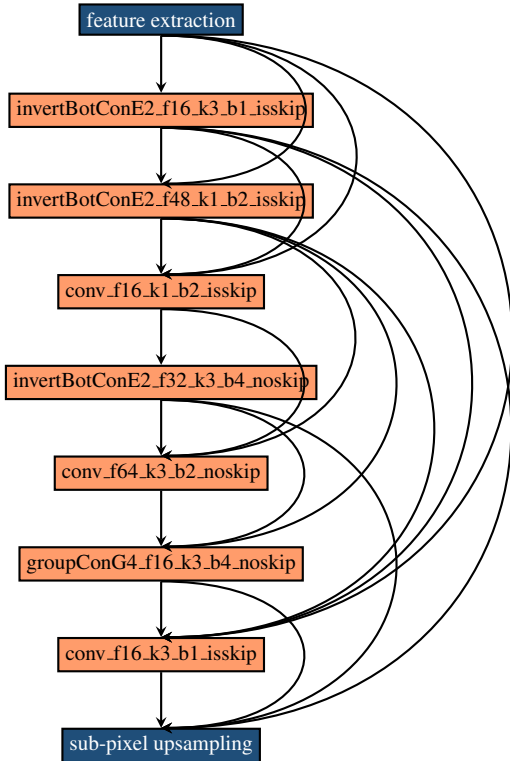


Figure 4: The model FALSR-B comparable to CARN-M.

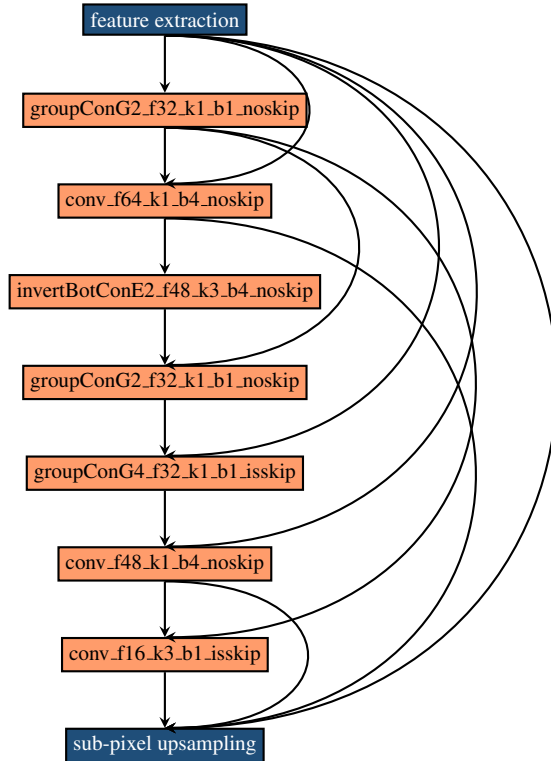


Figure 5: The model FALSR-C comparable to CARN-M

[He *et al.*, 2016] Kaiming He, Xiangyu Zhang, Shaoqing Ren, and Jian Sun. Deep residual learning for image recognition. In *Proceedings of the IEEE conference on computer vision and pattern recognition*, pages 770–778, 2016.

[Hore and Ziou, 2010] Alain Hore and Djemel Ziou. Image quality metrics: Psnr vs. ssim. In *Pattern recognition (icpr), 2010 20th international conference on*, pages 2366–2369. IEEE, 2010.

[Hsu *et al.*, 2018] Chi-Hung Hsu, Shu-Huan Chang, Da-Cheng Juan, Jia-Yu Pan, Yu-Ting Chen, Wei Wei, and Shih-Chieh Chang. Monas: Multi-objective neural architecture search using reinforcement learning. *arXiv preprint arXiv:1806.10332*, 2018.

[Kim *et al.*, 2016a] Jiwon Kim, Jung Kwon Lee, and Kyoung Mu Lee. Accurate image super-resolution using very deep convolutional networks. In *Proceedings of the IEEE conference on computer vision and pattern recognition*, pages 1646–1654, 2016.

[Kim *et al.*, 2016b] Jiwon Kim, Jung Kwon Lee, and Kyoung Mu Lee. Deeply-recursive convolutional network for image super-resolution. In *Proceedings of the IEEE conference on computer vision and pattern recognition*, pages 1637–1645, 2016.

[Lai *et al.*, 2017] Wei-Sheng Lai, Jia-Bin Huang, Narendra Ahuja, and Ming-Hsuan Yang. Deep laplacian pyramid networks for fast and accurate superresolution. In *IEEE*

Conference on Computer Vision and Pattern Recognition, volume 2, page 5, 2017.

[Lu *et al.*, 2018] Zhichao Lu, Ian Whalen, Vishnu Boddeti, Yashesh Dhebar, Kalyanmoy Deb, Erik Goodman, and Wolfgang Banzhaf. Nsga-net: A multi-objective genetic algorithm for neural architecture search. *arXiv preprint arXiv:1810.03522*, 2018.

[Ren *et al.*, 2017] Haoyu Ren, Mostafa El-Khamy, and Jungwon Lee. Image super resolution based on fusing multiple convolution neural networks. In *2017 IEEE Conference on Computer Vision and Pattern Recognition Workshops (CVPRW)*, pages 1050–1057. IEEE, 2017.

[Tai *et al.*, 2017a] Ying Tai, Jian Yang, and Xiaoming Liu. Image super-resolution via deep recursive residual network. In *Proceedings of the IEEE Conference on Computer Vision and Pattern Recognition*, volume 1, page 5, 2017.

[Tai *et al.*, 2017b] Ying Tai, Jian Yang, Xiaoming Liu, and Chunyan Xu. Memnet: A persistent memory network for image restoration. In *Proceedings of the IEEE Conference on Computer Vision and Pattern Recognition*, pages 4539–4547, 2017.

[Zhang *et al.*, 2018a] Yulun Zhang, Kunpeng Li, Kai Li, Lichen Wang, Bineng Zhong, and Yun Fu. Image super-resolution using very deep residual channel attention net-

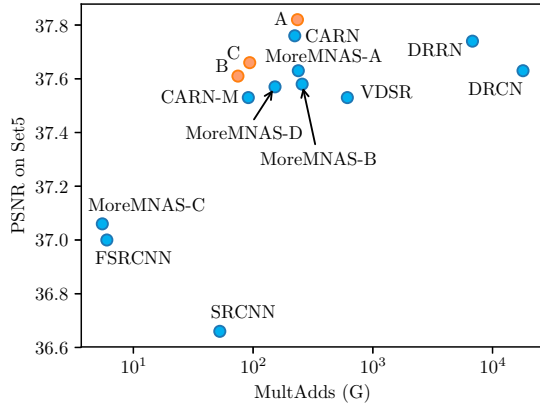


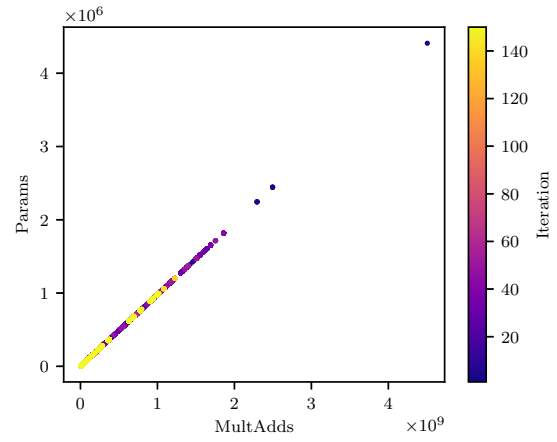
Figure 6: FALSRS A, B, C (shown in salmon) vs. others (light blue)

works. In *Proceedings of the European Conference on Computer Vision, Munich, Germany*, pages 8–14, 2018.

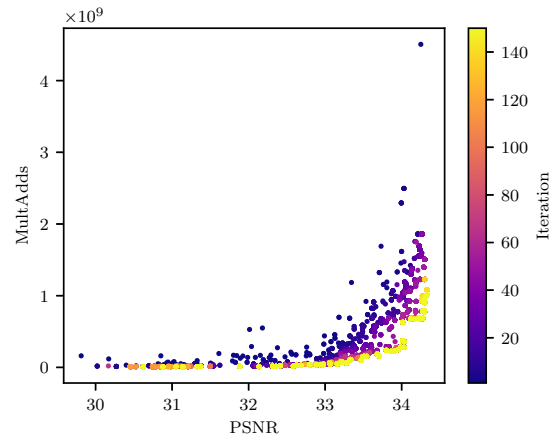
[Zhang *et al.*, 2018b] Yulun Zhang, Yapeng Tian, Yu Kong, Bineng Zhong, and Yun Fu. Residual dense network for image super-resolution. In *The IEEE Conference on Computer Vision and Pattern Recognition (CVPR)*, 2018.

[Zoph and Le, 2016] Barret Zoph and Quoc V Le. Neural architecture search with reinforcement learning. *arXiv preprint arXiv:1611.01578*, 2016.

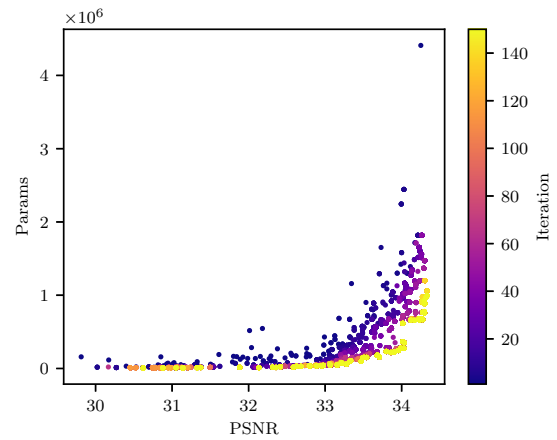
[Zoph *et al.*, 2017] Barret Zoph, Vijay Vasudevan, Jonathon Shlens, and Quoc V Le. Learning transferable architectures for scalable image recognition. *arXiv preprint arXiv:1707.07012*, 2(6), 2017.



(a)



(b)



(c)

Figure 7: Best models’s objectives during training.

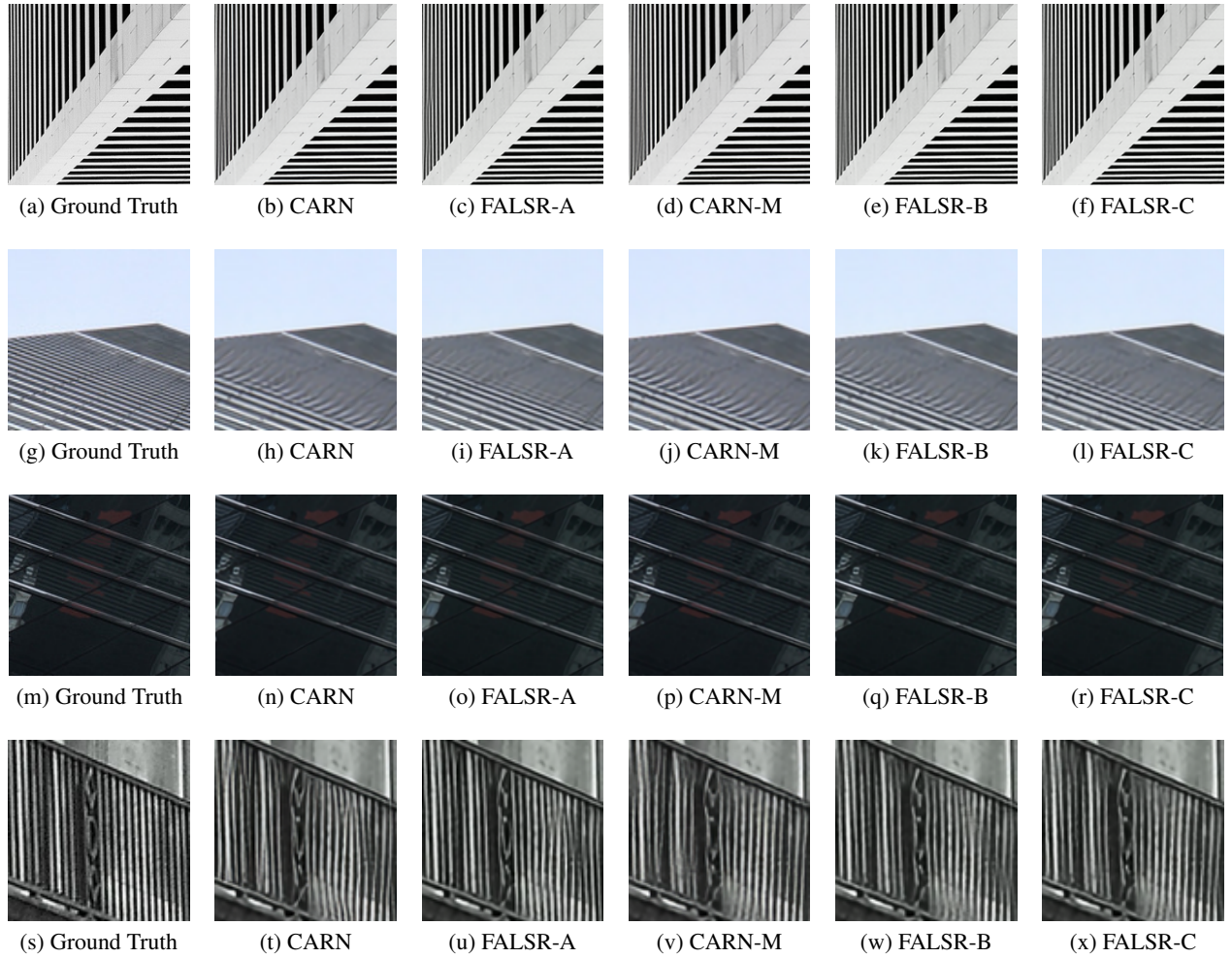


Figure 8: Qualitative results in comparison with others.